RSC Advances

Effect of synthesis routes on the properties and bactericidal activity of cryogels incorporated with silver nanoparticles

Journal:	*RSC Advances*
Manuscript ID:	RA-ART-05-2015-008449
Article Type:	Paper
Date Submitted by the Author:	07-May-2015

Complete List of Authors:	Loo, Siew-Leng; Singapore Membrane Technology Centre, Nanyang Technological University, ; School of Civil and Environmental Engineering, Nanyang Technological University, Krantz, William; Nanyang Technological University, Fane, Anthony; Nanyang Technological University, Hu, Xiao; Nanyang Technological University, School of Materials Sci & Eng Lim, Teik-Thye; Nanyang Technological University, Division of Environmental and Water Resources Engineering

Cite this: DOI: 10.1039/c0xx00000x

www.rsc.org/xxxxxx

ARTICLE TYPE

Effect of synthesis routes on the properties and bactericidal activity of cryogels incorporated with silver nanoparticles

Siew-Leng Loo,[ab] William B. Krantz,[ac] Anthony G. Fane,[ab] Xiao Hu*[ad], and Teik-Thye Lim*[ab]

Received (in XXX, XXX) Xth XXXXXXXXX 20XX, Accepted Xth XXXXXXXXX 20XX

DOI: 10.1039/b000000x

Incorporation of silver nanoparticles (AgNPs) into support materials has been demonstrated as an effective strategy to overcome issues related to particle aggregation and recovery. However, the properties of the resulting nanocomposites can be substantially different depending on the method used to incorporate the AgNPs into the support material. The support material chosen in this study is a poly(sodium acrylate) (PSA) cryogel that shows fast and substantial swelling as well as excellent mechanical properties. The objective of this paper was to compare the effects of employing different synthesis approaches on the properties and bactericidal activity of the resulting PSA/AgNP cryogels prepared via three synthesis routes: (i) incorporation of pre-synthesized AgNPs during cryogelation, (ii) ice-mediated coating of pre-synthesized AgNPs on pre-formed PSA cryogels, and (iii) *in situ* reduction of PSA cryogels loaded with Ag^+. The three synthesis methods resulted in PSA/AgNP cryogels with different AgNP-size and -spatial distributions, pore morphology, swelling and mechanical behavior, and disinfection efficacy. PSA/AgNP cryogels with a higher ratio of surface-bound Ag to bulk Ag content show significantly enhanced bactericidal activity that underscores the importance of considering the spatial distribution of AgNPs (in the support material) in the design of effective bactericidal nanomaterials.

1 Introduction

Various antimicrobial agents have been developed to combat microbiological contamination of potable water sources that threatens public health. Among them, silver in the form of a nanostructured material has been widely recognized as an excellent antimicrobial agent because of its broad-spectrum antimicrobial activity and low-toxicity to human cells.[1-3] The bactericidal effects of AgNPs (silver nanoparticles) include impairment of functional biomolecules such as enzymes, DNA, and membrane proteins through the action of dissolved Ag^+ ions and the physicochemical effects specific to the nanoparticles.[4-8] Fine AgNPs with higher specific surface area are usually preferred due to their enhanced bactericidal activity.[9-13] However, AgNPs tend to aggregate with a consequent decrease in their disinfection performance. Another practical issue to be addressed is the recovery and separation of the AgNPs from the treated water that may be time- and energy-consuming, and limits their reusability.

To address the aforementioned issues, a wide range of materials such as activated carbon, ceramic filters, hydrogels, cellulosic papers, polyurethane foams, resins, and rice husks have been employed to support AgNPs for water disinfection applications.[3,14-19] This strategy minimizes aggregation of the AgNPs and allows their simultaneous separation from the treated water since the AgNPs are retained in the support materials. Furthermore, the lifespan of the supported AgNPs can be enhanced due to controlled release of dissolved Ag^+ that enables long-term applications. However, one disadvantage of incorporating AgNPs in a dense support material is the possibility of reducing the accessibility of the AgNPs for interaction with the target bacteria. Therefore, in addition to being low-cost and robust, an ideal support material should have high porosity with micrometer-sized pores to allow enhanced cell-AgNP interaction. In addition, it would be advantageous if the support material could dynamically facilitate cell-AgNP interaction that would lead to enhanced disinfection rate. From operational perspectives, it is also crucial if the selected support material could enable a simple approach to recover the treated water while retaining AgNPs within its matrix.

The support material that possesses the aforementioned characteristics is a poly(sodium acrylate (PSA) cryogel, which is a macroporous hydrogel prepared via cryogelation.[20] In fact, polymeric cryogels such as alginate, chitosan, polyacrylamide, and poly(2-hydroxyethyl methacrylate) have been successfully used to support various nanomaterials.[21-24] PSA cryogels can be effective support materials for AgNPs because the interconnected micrometer-sized pores allow maximum accessibility to the bacterial cells. Furthermore, they have been shown to have fast and substantial swelling as well as excellent mechanical properties.[25] Because of its ability to rapidly imbibe water, this would drive the bacteria to flow into the cryogel whereby the bacteria can be exposed to the AgNPs supported on the pore

surface of the cryogels. In addition, the remarkable elasticity of cryogels enables them to be used as antibacterial sorbents whereby the disinfected water can be readily recovered via a simple squeezing step. The simplicity of this approach in combination of the lightweight of the cryogels suggest that they can be a fast-response solution to provide potable water in emergencies where there is limited access to the water supply infrastructure.[26]

A variety of different synthesis methods have been developed to incorporate nanoparticles in polymeric materials.[27] However, employing different synthesis methods is anticipated to result in a variation of structures that would affect the performance of the resultant nanocomposites. Therefore, the selection of an appropriate synthesis approach is crucial to fabricate materials with tailored properties to meet the requirements of a particular application. The focus of this paper was to compare the effects of synthesis methods on the material properties and bactericidal activity of AgNPs-incorporated PSA cryogels (or PSA/AgNP cryogels). In this study PSA/AgNP cryogels were prepared using three synthesis routes: (i) incorporation of pre-synthesized AgNPs during cryogelation, (ii) ice-mediated coating of pre-synthesized AgNPs on pre-formed PSA cryogels, and (iii) *in situ* reduction of PSA cryogels loaded with Ag^+. These methods are expected to result in varying spatial distribution of the AgNPs in the cryogels that could significantly influence the reactivity and bactericidal efficacy of the resultant cryogel nanocomposites.

2 Materials and methods

2.1 Preparation of AgNP stock suspension

Citrate-stabilized AgNPs suspensions were prepared following the method described by Jana et al. [28] with slight modifications. A 490-mL solution of 0.3 mM trisodium citrate and 1 mM of $NaBH_4$ was prepared in an ice bath; 10 mL of 10 mM $AgNO_3$ then was added into the reaction mixture and allowed to mix for 1 h. An *in situ* size-distribution of the as-synthesized citrate-stabilized AgNPs by dynamic light scattering (Malvern Zetasizer) revealed that the particles were mostly smaller than 10 nm (Supplementary Fig. S1). The mean diameter of the AgNPs was determined to be 24.2 ± 8.5 nm via analysis of TEM images (Supplementary Fig. S1). The citrate-stabilized AgNPs have a Zeta potential of -48.5 mV.

2.2 Preparation of PSA cryogels

The design principles and synthesis of PSA cryogels were previously described.[25] Briefly, ammonium persulfate (APS, 98% purity, Sigma-Aldrich) and *N,N,N',N'*-tetramethylethylenediamine (TEMED, ≥ 99%, Sigma-Aldrich) were added to a reaction mixture containing sodium acrylate (SA, 97%, Sigma-Aldrich) and *N,N'*-methylenebis(acrylamide) (MBA, 99%, Sigma-Aldrich), that was degassed and chilled in an ice bath. The APS and TEMED concentrations in the final reaction mixture were 1.75 mM and 8.4 μM, respectively. The monomer concentration (SA + MBA) used was 8% at a crosslinker ratio of 0.05 (mol MBA/mol SA). The resultant reaction mixture was transferred into several poly(propylene) syringes (3 mL and 9 mm ID) that were placed into a bath fluid (–20 °C, 1:1 mixture of ethylene glycol/MilliQ water (18.2 MΩ·cm at 25 °C)) incubated in an ultra-low temperature freezer (Eutra ED-FU4100). After 24 h, the PSA cryogels were thoroughly washed in MilliQ water and dehydrated in *t*-butanol followed by drying in a freeze-dryer (Alpha 1-4LD, –45 °C) before they were fractured into smaller cylindrical disk samples. The PSA cryogels had an ion-exchange capacity of 9.0 ± 0.8 meq/g as determined using the acid-base titration method described elsewhere.[29]

2.3 Preparation of PSA/AgNP cryogel nanocomposites

Three different synthesis routes were used to prepare PSA/AgNP cryogels that resulted in a variation in the AgNP-size and -spatial distribution in the PSA cryogels.

In the first method, the nanocomposites were fabricated by cryopolymerization of SA and MBA in the presence of the pre-formed citrate-stabilized AgNPs. The cryogelation conditions used were the same as those for PSA cryogels; the Ag concentration in the mixture was 0.2 mM. These nanocomposites will be subsequently referred to as NI (nanoparticle incorporated) cryogels.

The second method involved ice-mediated coating (IMC) of the pre-formed citrate-stabilized AgNPs on the PSA cryogels. 1 g of the dried PSA cryogels was allowed to swell in a 250 mL of the AgNP suspension (0.2 mM) with simultaneous shaking. After 24 h, the swollen cryogels were removed and placed in a freezer (–20 °C) for another 24 h. Care was taken to prevent accidental squeezing out of the absorbed AgNPs solution from the swollen cryogel. Hereafter, these nanocomposites is referred to as IMC cryogels.

The last method involved an intermatrix synthesis (IMS) method to prepare the PSA/AgNP cryogels. 1 g of the dried PSA cryogels was allowed to swell in a 250-mL solution of 0.2 mM of $AgNO_3$ (≥98%, Merck). The suspension was agitated at 120 rpm using an orbital shaker for 24 h in the dark. Then, the cryogels were immersed in a 250-mL solution of $NaBH_4$ (Alfa Aesar, 10:1 molar ratio of $NaBH_4$ to $AgNO_3$) for 1 h to AgNPs. The nanocomposites produced by this method are referred to as IMS cryogels.

All the resultant nanocomposites were thoroughly washed by immersion in MilliQ water followed by vacuum filtration. After three repetitions of the washing step, the nanocomposites were dried using the same procedure that was used for the PSA cryogels.

2.4 Characterization of PSA/AgNP cryogel nanocomposites

Field emission scanning electron microscopy (FESEM) was used to visualize the morphology of the cryogels. Prior to imaging, the samples were coated with Pt for 30 s (20 mA) using an auto-fine coater (JEOL JFC-1600). Elemental composition and distribution of the nanocomposites were examined using an energy-dispersive X-ray spectroscopy detector (EDX). The specific pore volumes of the cryogel nanocomposites were estimated by cyclohexane uptake as described elsewhere.[30] The topography of the nanocomposites was characterized using atomic force microscopy (AFM, XE-100, Park Systems, Korea) via the tapping mode in air at 26 °C. Note that thin hydrogel (nanocomposite) films were

used for the AFM studies. The AgNP morphology and size were studied using a transmission electron miscroscope (TEM, Carl Zeiss Libra 120) at an accelerating voltage of 120 kV; the particle-size distribution of the AgNPs was analyzed using image analysis software (ImageJ). A computer-controlled mechanical testing system (Instron 5567) was used to characterize the mechanical properties of the 10-mm thick fully-swollen nanocomposites at room temperature; a 5 kN load cell at a ramp-rate of 10 mm/min was used; the sample was compressed up to 95% strain based on its initial length. The swelling properties and water recoveries were determined by gravimetric analysis as described elsewehere.[25,31] The Ag incorporation efficiency was determined via gravimetric analysis of the transferral of Ag from the synthesis solution to the resultant PSA/AgNP cryogels.

2.5 Determination of disinfection efficacies of PSA/AgNP cryogel nanocomposites

The disinfection efficacies of the nanocomposites were studied using *Escherichia coli* (*E. coli,* ATCC® 25922™) as the model bacterium. *E. coli* was cultivated in tryptic soy broth at 37 °C to reach the mid-exponential growth phase. The cells were harvested by centrifugation followed by re-suspension in phosphate-buffered saline (PBS, 0.01 M, pH = 7.45) to form a bacterial suspension having a cell density of 10^8 colony-forming units per mL (cfu/mL). To determine the disinfection efficacies, the cryogel nanocomposites were used as sorbents to soak up a bacterial suspension allowing close contact between the *E. coli* cells and the interface of the cryogel nanocomposites. In a typical test, a cryogel disk sample (about 0.02 g) was allowed to swell a 10-mL bacterial suspension with manual shaking. Control experiments were also conducted using unmodified PSA cryogels. The swollen cryogels were immediately removed and squeezed to recover the absorbed water after being allowed to swell in the suspension for 15 s. The water squeezed out from the cryogels was diluted in PBS before plating the bacterial suspension on tryptic soy agar. The number of viable bacteria grown on the agar plate was determined after incubation for 24 h. The disinfection efficacies of the nanocomposites were also qualitatively assessed using fluorescence imaging of the exposed bacterial cells stained with SYTO 9 (6 mM) and propidium iodide (PI, 30 mM) (Live/Dead Baclight kit, Molecular Probes). Stained samples then were observed under an epifluorescence microscope (Olympus BX60) using a 100X oil objective at an excitation wavelength of 470 nm.

2.6 Analytical methods for Ag determination

The total Ag concentration in the solution sample (or digestate) was determined by using either an inductively coupled plasma-optical emission spectrophotometer (ICP-OES, Perkin Elmer Optima 2000DV) or an inductively coupled plasma-mass spectrometer (ICP-MS, Elan DRC-e) depending on the concentration range of the samples. Prior to analysis, all samples were prepared by close-vessel digestion in concentrated HNO_3 (65%) at 150 °C on a digestor unit (Hach DRB 200). For digestion of the cryogel nanocomposites, H_2O_2 (5%) was added to ensure complete solubilization. All experiments were conducted in triplicate.

3 Results and Discussion

3.1 Synthesis of PSA/AgNP cryogel nanocomposites

Fig. 1 summarizes the processes involved in the three synthesis routes used to fabricate PSA/AgNP cryogels with different Ag distributions. The fabrication of NI cryogels appears simple since it involved only one step, i.e., cryopolymerization of a physical mixture of monomer, crosslinker, and initiator in the presence of AgNPs. However, the formation of the PSA cryogel embedded with AgNPs is actually a complex process combining ice growth, nanoparticle embedding, and copolymerization occurring simultaneously (Fig. 1a). During freezing, the AgNPs are expelled from the growing ice crystals together with the monomer, crosslinker, and initiator in the confined unfrozen space between adjacent ice crystals. The AgNPs are entrapped within the pore walls of the cryogel as copolymerization between SA and MBA proceeds in the unfrozen liquid microphase (UFLP).[32] The pores are formed within the polymerized cryogel upon melting of the ice crystals. The presence of the AgNPs might have affected the cryogelation process because the gel fraction yield was significantly reduced (30% versus 95% without the AgNPs). Because the Ag concentration in the free water of the as-synthesized NI cryogel was very low (< 5 μg/L), it is reasonable to assume that most of the added AgNPs were embedded in the cryogels. Nonetheless, it should be noted that depending on the size of the AgNPs or their aggregates, they may be fully or partially embedded within the cryogel matrix as shown in the right-most panel of Fig. 1a. The Ag content of the NI cryogel was determined to be 0.8±0.3 mg/g. Note that the Ag content in the NI cryogel is dictated not only by the Ag incorporation efficiency but also by the gel fraction yield.

On the other hand, the IMC and IMS cryogels were prepared using pre-formed PSA cryogels (with a gel yield of 95%) that allow a better control of the amount of Ag incorporated into the resulting composite. The unmodified PSA cryogels are highly porous with well-interconnected pore channels (Fig. 2a). This allow unhindered diffusion of solutes rendering their pores to be easily filled with AgNPs upon immersion in the nanoparticle suspension. As depicted in Fig. 1b, the subsequent freezing step in the IMC method induced nucleation and growth of ice crystals that propels the AgNPs away from the ice front to reduce the surface energy.[33-37] This additional freezing step assists the deposition and assembly of AgNPs on the pore surface in the PSA cryogels. Compared to the PSA/AgNP cryogels prepared without the post-freezing step, the Ag incorporation efficiency was significantly enhanced; it increased from 4.6±0.6% to 26.0±3.8% with the additional freezing step. Without the additional freezing step, most of the absorbed AgNPs were released back into solution during washing (Supplementary Fig. S2). The Ag content of the as-synthesized IMC cryogel was 1.4±0.2 mg/g.

As illustrated in Fig. 1c, the fabrication of the IMS cryogels involves (i) loading of the pre-formed PSA cryogels with Ag^+ ions via an ion-exchange reaction followed by (ii) reduction of the sorbed Ag^+ ions by $NaBH_4$.[38] Both reactions are represented as eqns (1) and (2), respectively :

$$R–COO^- Na^+ + Ag^+ \rightarrow R–COO^- Ag^+ + Na^+ \quad (1)$$

$$R–COO^- Ag^+ + NaBH_4 + 3H_2O \rightarrow R–COO^- Na^+ + Ag^0 + 3.5H_2 + B(OH)_3 \quad (2)$$

Due to its high ion-exchange capacity (i.e., 9.0±0.8 meq/g) and high affinity of the $–COO^-$ groups towards Ag^+, all the Ag^+ can be rapidly taken up in the first step. As such, cryogels with higher Ag content can be readily prepared by increasing the concentration of precursor Ag^+. However, the Ag incorporation efficiency was only 74.8±2.7% because a portion of the sorbed Ag^+ ions was released back into the solution during the second step driven by the Ag concentration gradient between cryogel and the bulk solution. The IMS cryogels had an Ag content of 4.0±0.2 mg/g.

The NI and IMC cryogels were prepared using pre-formed AgNPs that allows the flexibility of using commercially available AgNPs. However, a key problem could be the limited dispersibility of the AgNPs, especially at high concentrations that might preclude the preparation of nanocomposites having a high Ag content. Although the NI method has the highest Ag incorporation efficiency, the amount of Ag incorporated also depends on the gel fraction yield that makes the control and prediction of Ag content in the resultant nanocomposite difficult. In contrast, the IMS method requires *in situ* reduction to form AgNPs but allows the preparation of high Ag content and better control of the amount of Ag incorporated.

3.2 Characteristics of PSA/AgNP cryogel nanocomposites

For the IMS and IMC cryogels, the incorporation of AgNPs into the pre-formed PSA cryogels did not cause any significant change in the pore structure of the cryogel as evidenced by their SEM images (Fig. 2c and d). In fact, both the IMS and IMC cryogels show a slight increase in their specific pore volumes relative to the PSA cryogels (Table 1). The increased pore volumes for the IMS and IMC cryogels might be due to the repulsion between the electron-dense AgNPs that causes expansion of the network and/or pores of the cryogels. In contrast, the NI cryogels prepared by cryogelation in the presence of AgNPs show a significant reduction in porosity compared to the PSA cryogels (Table 1). Furthermore, the SEM image of an NI cryogel shows the lack of open pores (Fig. 2b). Note that to obtain cryogels with well-interconnected pore channels, the conditions for cryogelation (i.e., reagent concentration and freezing temperature among others) must be precisely controlled to ensure that freezing occurs before gelation. The lack of open pores in the case of the NI cryogels might be due to an increased viscosity (due to the presence of additional AgNPs) in the unfrozen liquid microphase that reduces the freezing rate and thereby prevents the ice crystals from merging into the gelled mixture.[25] A similar observation has also been made by Seo et al. when preparing cryogel nanocomposites via this method.[39]

One of the main motivations for stabilizing the AgNPs in the support materials was to prevent their aggregation in order to maintain their small size; smaller-sized particles have been found to display superior bactericidal efficacy.[9-11] Interestingly, the AgNPs incorporated into cryogels via different methods have distinctly different sizes (Fig. 3). The mean AgNP sizes for the NI, IMC, and IMS cryogels were determined to be 25.1±13.4, 12.2±8.5, and 5.7±2.1 nm, respectively (Table 1). Notably, the mean size of the AgNPs in the IMS cryogels is significantly smaller than those of the NI and IMC cryogels. This is mainly due to the *in situ* reduction of Ag^+ stabilized on the PSA cryogel matrix that bypasses aggregation problems encountered when using nanoparticle suspensions for synthesis. Furthermore, the free volume in the highly crosslinked network of PSA can provide spatial confinement for the growing AgNPs resulting in the formation of ultrafine particles.[40-43]

Besides AgNP size, the spatial distribution of the AgNPs in the support material may also influence the bactericidal efficacy of the resultant nanocomposites. To verify the location of AgNPs in the cryogel matrix, topographic studies using AFM were conducted along with EDX analyses of the cryogel surfaces (Fig. 4). The AFM image of the control (i.e., without AgNP incorporation) shows a smooth topography (Supplementary Fig. S3). For the NI cryogels the AgNPs are expected to be embedded throughout the polymer matrix of the NI cryogels. This hypothesis is supported by the low surface Ag content and a relatively smooth topography (Fig. 4). Nevertheless, some large AgNP clusters protruding from the gel surface can be observed in the AFM image that causes an increase in the surface roughness relative to the unmodified gel (Fig. 4a and Table 1). Note that although the AgNPs are generally embedded within the pore wall of the NI cryogel, some of them, in particular the larger-sized AgNP clusters, may only be partially embedded as illustrated in Fig. 1a. Therefore, the increase in surface roughness may be attributed to the protrusion of partially embedded particles rather than a "real" surface distribution of AgNPs (Table 1). It has been found that scaffolds prepared in the presence of small particles (6 nm) formed featureless pore walls with concealed particles, whereas when larger particles (25 nm) were used they remained exposed at the surface of the channel walls.[24] In contrast, the IMC cryogels had the AgNPs located only on their pore surfaces because the AgNPs could not penetrate the dense PSA matrix due to steric hindrance. This hypothesis is supported by the significant increase in surface roughness and the presence of AgNP clusters on the surface that are apparent in both the AFM and FESEM images (Fig. 4a and b). Furthermore, EDX analyses revealed that the majority of the pore surfaces show an intense signal for surface-bound Ag (27-43 wt%). However, the IMS cryogel, show an Ag distribution that has features of that observed in the NI and IMC cryogels whereby the AgNPs are incorporated throughout the cryogel matrix but with the majority of the AgNPs being located on the pore surfaces. As illustrated in Fig. 1c, this is the result of Donnan exclusion effect during the second step of IMS (i.e., reduction of the Ag^+ sorbed on PSA cryogel) whereby BH_4^- is unable to diffuse deeply into the PSA matrix due to electrostatic repulsion between the negatively charged surface cryogels and BH_4^- resulting in the formation of AgNPs primarily on the exposed pore surfaces.[44] As such, the surface of the pore walls of the IMS cryogels appear to be densely decorated with AgNPs as evidenced by their AFM and FESEM images (Fig. 4b and c). Despite the peripheral distribution and higher Ag content of the IMS cryogels, the surface-bound Ag was significantly lower than that of IMC cryogels (6-15%). Although the majority of the AgNPs were

located on the surface of IMS cryogel, only a small increase in the surface roughness was observed that may be attributed to the small size of the AgNPs on the surface (Table 1 and Fig. 4a).

The difference in the morphology and Ag distribution among the NI, IMC, and IMS cryogels is expected to result in distinctly different bulk properties such as their swelling-deswelling and mechanical properties. Note that in order to be applied as antibacterial sorbents for water disinfection, the cryogels should preferably have fast and high water absorption and desorption. Furthermore, the cryogels should have a high elasticity and durability to allow repeated use. Similar to the PSA cryogels, both the IMC and IMS cryogels can reach swelling degrees greater than 150 g/g within 15 s due to the highly interconnected pore channels (Fig. 5a and b). Furthermore, 85% of their absorbed water can be recovered using mild pressure compression (Fig. 5c). However, due to the presence of closed pores and reduced porosity, the NI cryogels could only swell to 76.3±7.9 g/g (also within 15 s, but with a slight decrease in the swelling rate with respect to the PSA cryogel); moreover, the water recovery was reduced to 72% (Fig. 5c). Nonetheless, the incorporation of AgNPs has provided some form of reinforcement to the mechanical structure of the NI cryogels and to a lesser extent the IMS cryogels as evidenced by their increased Young's modulus relative to the PSA cryogels (Fig. 6). The increased stiffness of the NI and IMS cryogels may be attributed to extensive integration of the AgNPs into the polymer matrix that could hinder buckling of the polymer chains when placed under compression.[24] Although the NI cryogels show the highest enhancement in terms of the Young's modulus, the large hysteresis loop indicates a substantial loss of elasticity that may be undesirable for application as antibacterial sorbents (Fig. 6). This loss of elasticity may be attributed to the presence of closed pores and the reduced porosity of the NI cryogels. On the other hand, there is no mechanical reinforcement for the IMC cryogels because the AgNPs are not incorporated within their matrix. In fact, there is a slight — but insignificant — reduction in the Young's modulus (compared to the PSA cryogel) owing to the additional freezing step that could have affected the structure of the polymer matrix due to the pressure exerted by the ice crystals against the pore walls (Fig. 6).

3.3 Application of the cryogel nanocomposites for POU water disinfection

The bactericidal efficacy of the as-synthesized NI, IMC, and IMS cryogels was determined by applying them as antibacterial sorbents to disinfect water. In this application, the cryogels were used to soak up bacterial suspension during which the bacterial cells enter the pores of the cryogels to effect disinfection. The disinfected water then can be recovered by squeezing the cryogels. Fig. 7 shows a qualitative comparison of the disinfection efficacies of the NI, IMC, and IMS cryogels with respect to the unmodified PSA cryogel via fluorescence imaging of exposed cells stained with dyes. Note that SYTO 9 is a permeant dye that stains all bacterial cells while propidium iodide (PI) is a non-permeant dye that can be taken up only by membrane-compromised cells. Therefore, viable cells fluoresce green while cells with a compromised membrane fluoresce red (since more PI can enter damaged cells) due to fluorescence quenching of SYTO 9 by PI. In contrast to PSA cryogels, bacterial cells exposed to NI, IMS, and IMC cryogels show cell-membrane damage albeit to varying degrees of severity (Fig. 7). The extent of cell-membrane damage of the cells exposed to the NI cryogels appears to be drastically less severe than those exposed to the IMC and IMS cryogels.

To obtain a more quantitative comparison, the bacterial suspension squeezed out from the different cryogels was plated and subsequently counted to determine the concentration of surviving cells. As shown in Fig. 8a, the results are consistent with the fluorescence images of the exposed cells. Both the PSA and NI cryogels result in a slight reduction of viable cells (Fig. 8a). While true inactivation of bacterial cells may apply for the case of the NI cryogels, the insignificant reduction in the number of viable cells for the case of the PSA cryogels is probably due serendipitous removal via physical mechanisms such as (i) bacterial exclusion by smaller pores, (ii) bacterial entrapment in blind pores, and/or (iii) deposition of bacterial cells on the interior surface of the cryogel during squeezing. In contrast, both the IMC and IMS cryogels show significant inactivation of bacterial cells whereby they can achieve 4.1±0.2 and 3.2±0.1 logs reduction, respectively. Notably, the IMC cryogels show the highest disinfection efficacy among the three nanocomposites. This is rather surprising because the IMC cryogels have a lower Ag release (42.8±2.5 µg/L versus 102.2±1.4 µg/L) and Ag content (1.4±0.2 mg/g versus 4.0±0.2 mg/g), and generally larger AgNPs than those of the IMS cryogels (Table 1).

As shown in Fig. 8b, the disinfection efficacy of the AgNPs incorporated into the cryogels shows a better correlation with the concentration of Ag on the cryogel surface rather than in the bulk of the cryogel. These results suggest that the location of the AgNPs is an important — and can be an overriding — factor in dictating the bactericidal efficacy of Ag-based nanocomposites. Therefore, to attain a superior bactericidal efficacy, AgNPs should be located on the pore surface rather than being embedded in the support material to allow maximum exposure to the bacterial cells. This is in line with the observations that bactericidal activity is enhanced with improved contact between the cells and the composite materials.[45-47]

Table 2 provides a summary of the merits and drawbacks of the synthesis methods explored in this study. The findings in the present study stress the importance of optimizing the synthesis approach to obtain desirable Ag-loaded nanocomposite properties to meet the requirements of a particular application. However, the choice of the optimal synthesis method is usually not only determined by the performance of the resulting material, but by a trade-off with other factors such as the ease of synthesis and upscalability among others. For example, even though the IMC resulted in cryogels with a higher disinfection efficacy, the IMS method may be a better option to prepare PSA/AgNP cryogels for application as antibacterial sorbents considering the reproducibility and ease of synthesis in addition to good antibacterial activity. Furthermore, mass production of PSA/AgNP cryogels via this method is more feasible.

4 Conclusions

PSA/AgNP cryogel nanocomposites were successfully prepared using three different synthesis approaches. The three synthesis

methods resulted in PSA/AgNP cryogels with distinctly different Ag distribution whereby the AgNPs were located only on the pore surface or embedded throughout the polymer matrix or a combination of both. Furthermore, the PSA/AgNP cryogels prepared via different methods have varying AgNP size, pore morphology, swelling and mechanical behavior. The three types of PSA/AgNP cryogels were found to be effective in disinfecting the *E. coli* to different extents. Specifically, synthesis routes that formed more AgNPs on the exterior surface of the cryogels displayed enhanced bactericidal efficacy. These findings suggests the importance of optimizing the synthesis approach to obtain material structures that lead to the desirable properties.

Acknowledgments

This project was conducted in the Singapore Membrane Technology Centre that is supported by the Economic Development Board of Singapore and is part of the Nanyang Environment and Water Research Institute at Nanyang Technological University. S.-L. Loo has been supported by the National Research Foundation Singapore under its National Research Foundation (Environment and Water Technologies) PhD Scholarship program, administered by the Environment and Water Industry of Singapore. The authors thank Ms. Maria Chong and Ms. Pearlyn Shee for their assistance with the FESEM and AFM analyses. The characterization studies were conducted at the Facility for Analysis, Characterization, Testing and Simulation (FACTS), and Central Environment Science and Engineering Laboratory (CESEL) at NTU.

Notes and references

[a]*Singapore Membrane Technology Centre, Nanyang Environment and Water Research Institute, Nanyang Technological University, 1 Cleantech Loop, CleanTech One, #05-05, Singapore 637141, Singapore.*

[b]*School of Civil and Environmental Engineering, Nanyang Technological University, Block N1, 50 Nanyang Avenue, Singapore 639798, Singapore. Email: cttlim@ntu.edu.sg; Tel.: +65 67906933; Fax: +65 67910676*

[c]*Department of Chemical and Biological Engineering, University of Colorado, Boulder, Colorado 80309-0424, USA.*

[d]*School of Materials Science and Engineering, Nanyang Technological University, Singapore 639798, Singapore. Email: ASXHU@ntu.edu.sg; +65 67904610; Fax: +65 68909081.*

† Electronic Supplementary Information (ESI) available: [Additional experimental results (Figs. S1-S3)]. See DOI: 10.1039/b000000x/

1. L. Balogh, D. R. Swanson, D. A. Tomalia, G. L. Hagnauer and A. T. McManus, *Nano Letters*, 2000, **1**, 18-21.
2. J. Liu, Z. Wang, F. D. Liu, A. B. Kane and R. H. Hurt, *ACS Nano*, 2012, **6**, 9887-9899.
3. A. Alonso, X. Muñoz-Berbel, N. Vigués, R. Rodríguez-Rodríguez, J. Macanás, M. Muñoz, J. Mas and D. N. Muraviev, *Advanced Functional Materials*, 2013, **23**, 2450-2458.
4. A. Nel, T. Xia, L. Mädler and N. Li, *Science*, 2006, **311**, 622-627.
5. A. K. Suresh, D. A. Pelletier and M. J. Doktycz, *Nanoscale*, 2013, **5**, 463-474.
6. S. Eckhardt, P. S. Brunetto, J. Gagnon, M. Priebe, B. Giese and K. M. Fromm, *Chemical Reviews*, 2013, **113**, 4708-4754.
7. L. Rizzello and P. P. Pompa, *Chemical Society Reviews*, 2014, **43**, 1501-1518.
8. J. A. Lemire, J. J. Harrison and R. J. Turner, *Nat Rev Micro*, 2013, **11**, 371-384.
9. O. Choi and Z. Hu, *Environmental Science & Technology*, 2008, **42**, 4583-4588.
10. S. Pal, Y. K. Tak and J. M. Song, *Applied and Environmental Microbiology*, 2007, **73**, 1712-1720.
11. J. R. Morones, J. L. Elechiguerra, A. Camacho, K. Holt, J. B. Kouri, J. T. Ramírez and M. J. Yacaman, *Nanotechnology*, 2005, **16**, 2346.
12. H. Zhang and V. Oyanedel-Craver, *Journal of Environmental Engineering*, 2012, **138**, 58-66.
13. A. Panáček, L. Kvítek, R. Prucek, M. Kolář, R. Večeřová, N. Pizúrová, V. K. Sharma, T. j. Nevěčná and R. Zbořil, *The Journal of Physical Chemistry B*, 2006, **110**, 16248-16253.
14. T. A. Dankovich and D. G. Gray, *Environmental Science & Technology*, 2011, **45**, 1992-1998.
15. S. Lin, R. Huang, Y. Cheng, J. Liu, B. L. T. Lau and M. R. Wiesner, *Water Research*, 2013, **47**, 3959-3965.
16. P. Jain and T. Pradeep, *Biotechnology and Bioengineering*, 2005, **90**, 59-63.
17. V. A. Oyanedel-Craver and J. A. Smith, *Environmental Science & Technology*, 2007, **42**, 927-933.
18. D. Gangadharan, K. Harshvardan, G. Gnanasekar, D. Dixit, K. M. Popat and P. S. Anand, *Water Research*, 2010, **44**, 5481-5487.
19. L. R. Pokhrel, B. Dubey and P. R. Scheuerman, *Environmental Science & Technology*, 2013, **47**, 12877-12885.
20. V. I. Lozinsky, *Russian Chemical Reviews*, 2002, **71**, 489-511.
21. I. N. Savina, C. J. English, R. L. D. Whitby, Y. Zheng, A. Leistner, S. V. Mikhalovsky and A. B. Cundy, *Journal of Hazardous Materials*, 2011, **192**, 1002-1008.
22. K. Yao, S. Shen, J. Yun, L. Wang, F. Chen and X. Yu, *Biochemical Engineering Journal*, 2007, **36**, 139-146.
23. K. Yao, J. Yun, S. Shen, L. Wang, X. He and X. Yu, *Journal of Chromatography A*, 2006, **1109**, 103-110.
24. C. Suwanchawalit, A. J. Patil, R. K. Kumar, S. Wongnawa and S. Mann, *Journal of Materials Chemistry*, 2009, **19**, 8478-8483.
25. S.-L. Loo, W. B. Krantz, T.-T. Lim, A. G. Fane and X. Hu, *Soft Matter*, 2013, **9**, 224-234.
26. S.-L. Loo, A. G. Fane, W. B. Krantz and T.-T. Lim, *Water Research*, 2012, **46**, 3125-3151.
27. P. Dallas, V. K. Sharma and R. Zboril, *Advances in Colloid and Interface Science*, 2011, **166**, 119-135.
28. N. R. Jana, L. Gearheart and C. J. Murphy, *Chemical Communications*, 2001, 617-618.
29. S. Fisher and R. Kunin, *Analytical Chemistry*, 1955, **27**, 1191-1194.
30. F. Topuz and O. Okay, *Reactive and Functional Polymers*, 2009, **69**, 273-280.
31. F. M. Plieva, M. Karlsson, M.-R. Aguilar, D. Gomez, S. Mikhalovsky and I. Y. Galaev, *Soft Matter*, 2005, **1**, 303-309.
32. P. Petrov, E. Petrova and C. B. Tsvetanov, *Polymer*, 2009, **50**, 1118-1123.
33. P. D. Petrov and G. L. Georgiev, *Chemical Communications*, 2011, **47**, 5768-5770.
34. S. Deville, E. Saiz, R. K. Nalla and A. P. Tomsia, *Science*, 2006, **311**, 515-518.
35. M. C. Gutiérrez, M. L. Ferrer and F. del Monte, *Chemistry of Materials*, 2008, **20**, 634-648.
36. L. Estevez, A. Kelarakis, Q. Gong, E. H. Da'as and E. P. Giannelis, *Journal of the American Chemical Society*, 2011, **133**, 6122-6125.
37. P. D. Petrov and G. L. Georgiev, *European Polymer Journal*, 2012, **48**, 1366-1373.
38. P. Ruiz, M. Muñoz, J. Macanás and D. N. Muraviev, *Chemistry of Materials*, 2010, **22**, 6616-6623.
39. S. Y. Seo, G. H. Lee, S. G. Lee, S. Y. Jung, J. O. Lim and J. H. Choi, *Carbohydrate Polymers*, 2012, **90**, 109-115.
40. Y. M. Mohan, T. Premkumar, K. Lee and K. E. Geckeler, *Macromolecular Rapid Communications*, 2006, **27**, 1346-1354.
41. P. S. K. Murthy, Y. Murali Mohan, K. Varaprasad, B. Sreedhar and K. Mohana Raju, *Journal of Colloid and Interface Science*, 2008, **318**, 217-224.
42. S. Agnihotri, S. Mukherji and S. Mukherji, *Appl Nanosci*, 2012, **2**, 179-188.
43. V. Kozlovskaya, E. Kharlampieva, S. Chang, R. Muhlbauer and V. V. Tsukruk, *Chemistry of Materials*, 2009, **21**, 2158-2167.

44. A. Alonso, J. MacAnás, A. Shafir, M. Muñoz, A. Vallribera, D. Prodius, S. Melnic, C. Turta and D. N. Muraviev, *Dalton Transactions*, 2010, **39**, 2579-2586.
45. S.-L. Loo, A. G. Fane, T.-T. Lim, W. B. Krantz, Y.-N. Liang, X. Liu and X. Hu, *Environmental Science & Technology*, 2013, **47**, 9363-9371.
46. S. Agnihotri, S. Mukherji and S. Mukherji, *Nanoscale*, 2013, **5**, 7328-7340.
47. O. Bondarenko, A. Ivask, A. Käkinen, I. Kurvet and A. Kahru, *PLoS ONE*, 2013, **8**, e64060.

List of Tables

List of Figures

Table 1 Salient properties of the cryogels prepared via different methods

Samples	Ag incorporation[a] (%)	Ag content (mg/g)	Specific pore volume[b] (cm^3/g)	Total Ag in squeezed water (μg/L)	Mean AgNP size[c] (nm)	Surface roughness[d] R(a) (nm)
PSA cryogel	N.A.	N.A.	2.8 (0.2)	N.A.	N.A.	4.4 (1.2)
NI cryogel	> 99	0.8 (0.3)	1.6 (0.1)	33.7 (0.7)	25.1 (13.4)	7.2 (2.7)
IMC cryogel	26.0 (3.8)	1.4 (0.2)	3.6 (0.1)	42.8 (2.5)	12.2 (8.5)	13.8 (1.4)
IMS cryogel	74.8 (2.7)	4.0 (0.2)	2.9 (0.2)	102.2 (1.4)	5.1 (2.1)	7.0 (1.5)

Note: N.A. = not applicable; standard deviations are shown in parentheses.

[a] The Ag incorporation efficiency was determined by taking the ratio of the mass of Ag incorporated into the cryogel nanocomposites to the mass of Ag in the initial synthesis solution.

[b] The specific pore volume was computed by measuring the mass increase of a cryogel immersed in cyclohexane (0.779 g/cm^3) versus its initial dry mass.

[c] Determined from TEM images.

[f] Determined from AFM images.

Table 2 Summary of advantages and the disadvantages of the synthesis approaches employed in this study

Synthesis approach	Advantages	Disadvantages
Cryogelation in the presence of pre-synthesized nanoparticles	• Low AgNP wastage due to high efficiency of Ag incorporation; • One-step synthesis; • Low Ag leaching; • Forms more robust cryogel nanocomposites.	• Difficult to control the Ag content in the resultant cryogel nanocomposite; • Need re-optimization of cryogelation conditions for synthesis of cryogels with different Ag contents; • The resultant nanocomposites have lower swelling rates and degree, elasticity, and water recovery; • Low bactericidal efficacy.
Ice-mediated coating of nanoparticles on pre-formed cryogels	• Can achieve high bactericidal efficacy at lower Ag content; • Low Ag leaching • Can use pre-formed cryogels with optimized swelling/deswelling and mechanical properties • Re-optimization of cryogelation conditions for synthesis of cryogels with different Ag contents not required.	• High wastage of AgNPs due to low efficiency of Ag incorporation - especially in the first step; • Difficult to prepare nanocomposites with high Ag content due to dispersion problems; • The post-freezing step may affect the mechanical properties of the resulting nanocomposites; • Multistep synthesis.
In situ reduction of nanoparticles on pre-formed cryogels	• Can achieve good bactericidal efficacy; • Can use pre-formed cryogels with optimized swelling/deswelling and mechanical properties • Re-optimization of cryogelation conditions for synthesis of cryogels with different Ag contents not required; • Can prepare cryogels with high and predictable Ag content; • Ag reloading of used cryogels possible; • Lower Ag wastage due to the higher Ag incorporation efficiency.	• Ag leaching higher than the other two methods; • Multistep synthesis.

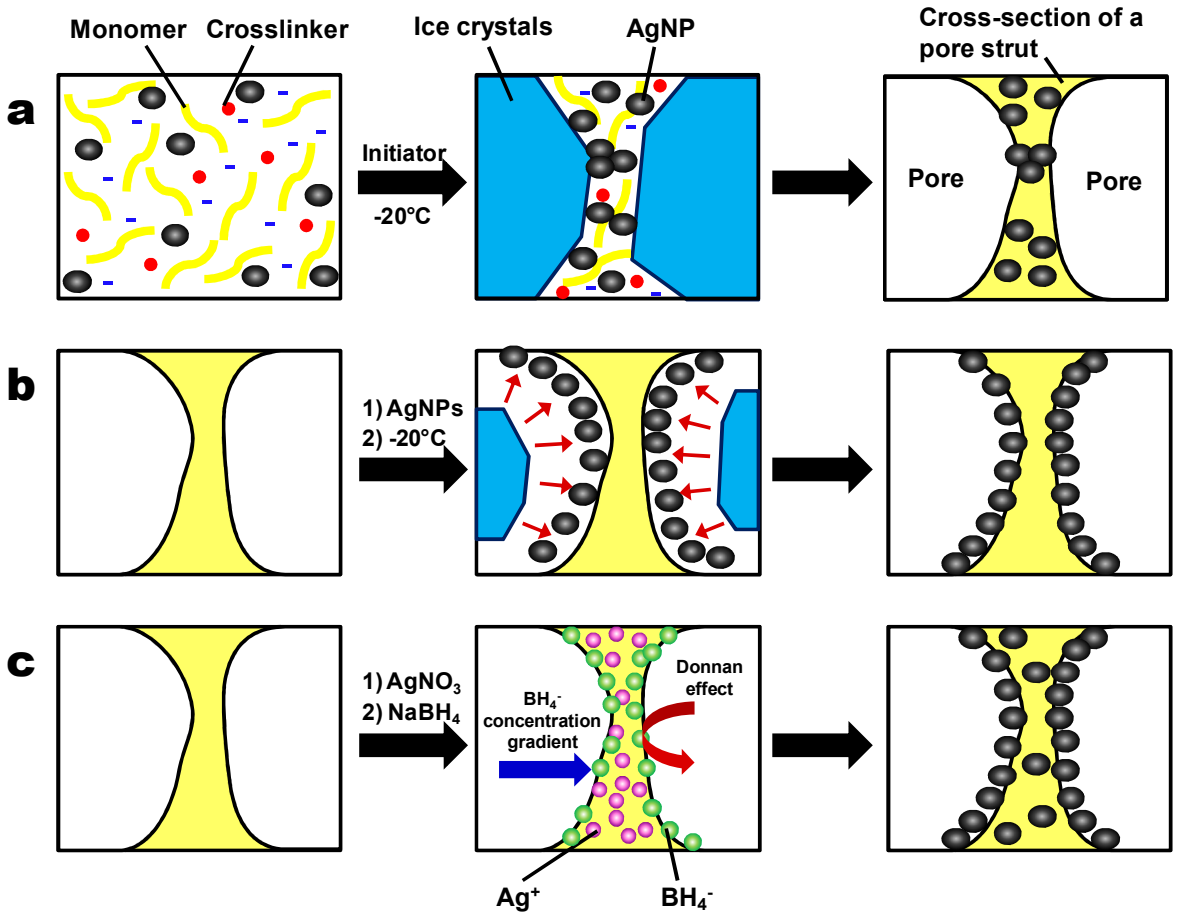

Fig. 1 Schematic diagram of the synthesis routes used to prepare (a) NI cryogels via cryogelation in the presence of pre-formed AgNPs, (b) IMC cryogels via ice-mediated coating of AgNPs on pre-formed PSA cryogels, and (c) IMS cryogels via *in situ* borohydride reduction of pre-formed PSA cryogels loaded with Ag^{+}; BH_4^{-} diffusion into the pore strut is driven by the concentration gradient at the interface of pore strut and bulk solution, but hindered by an opposing force due to Donnan exclusion effect.

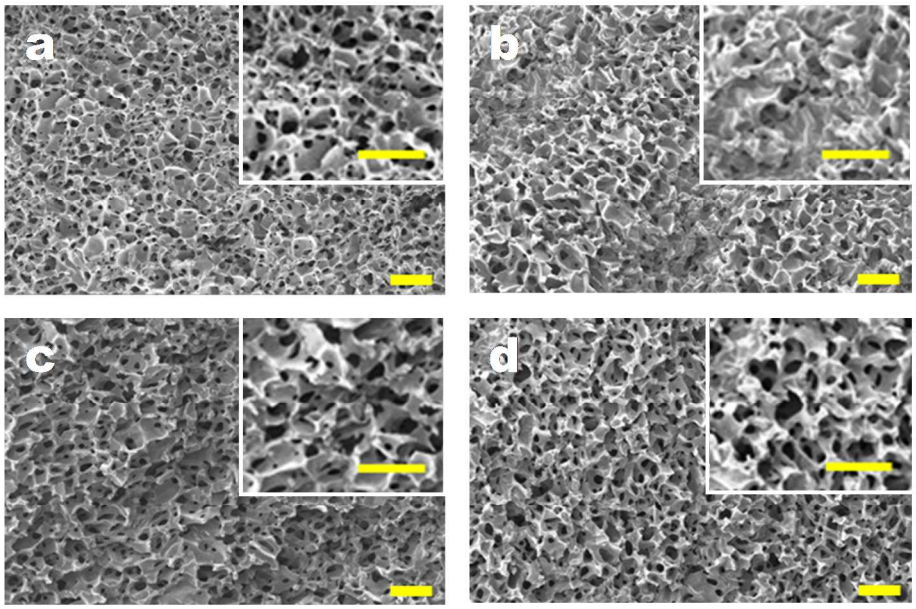

Fig. 2 SEM images depicting the morphologies of (a) PSA cryogels, (b) NI cryogels, (c) IMC cryogels, and (d) IMS cryogels. Note: scale bars represent 100 μm.

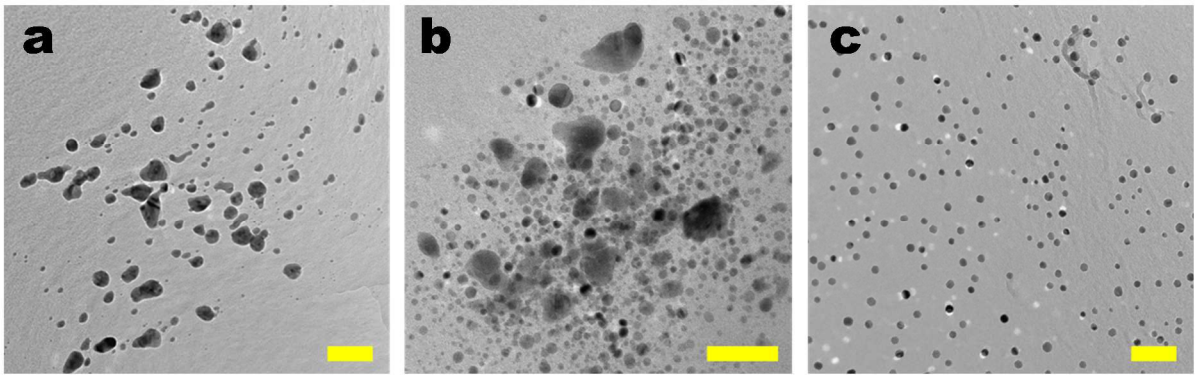

Fig.3 TEM images of the AgNPs incorporated in (a) NI, (b) IMC, and (c) IMS cryogels. Note: scale bars represent 50 nm.

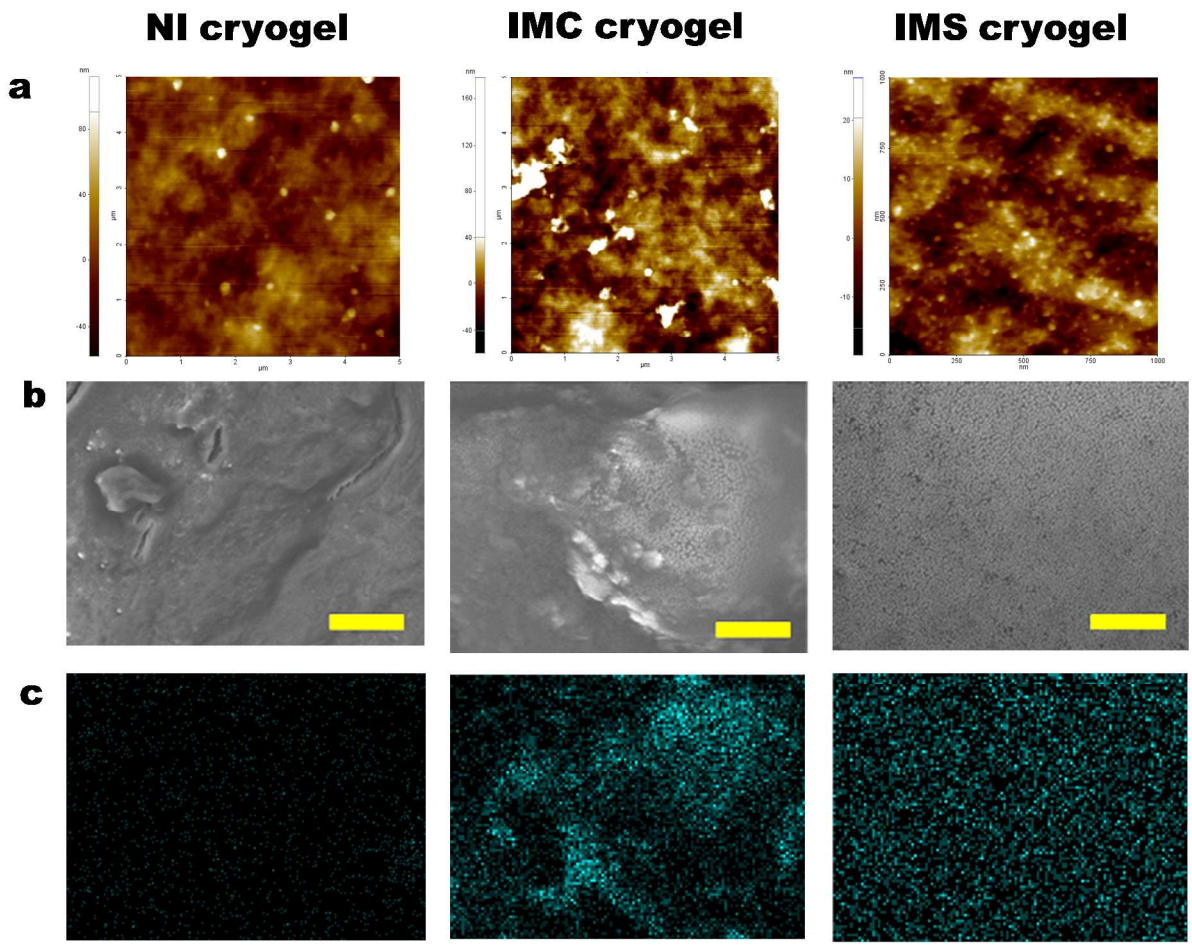

Fig. 4 Representative images from (a) AFM, (b) FESEM, and (c) EDX elemental Ag mapping of NI, IMC, and IMS cryogels. Note: scale bars in (b) represent 500 nm.

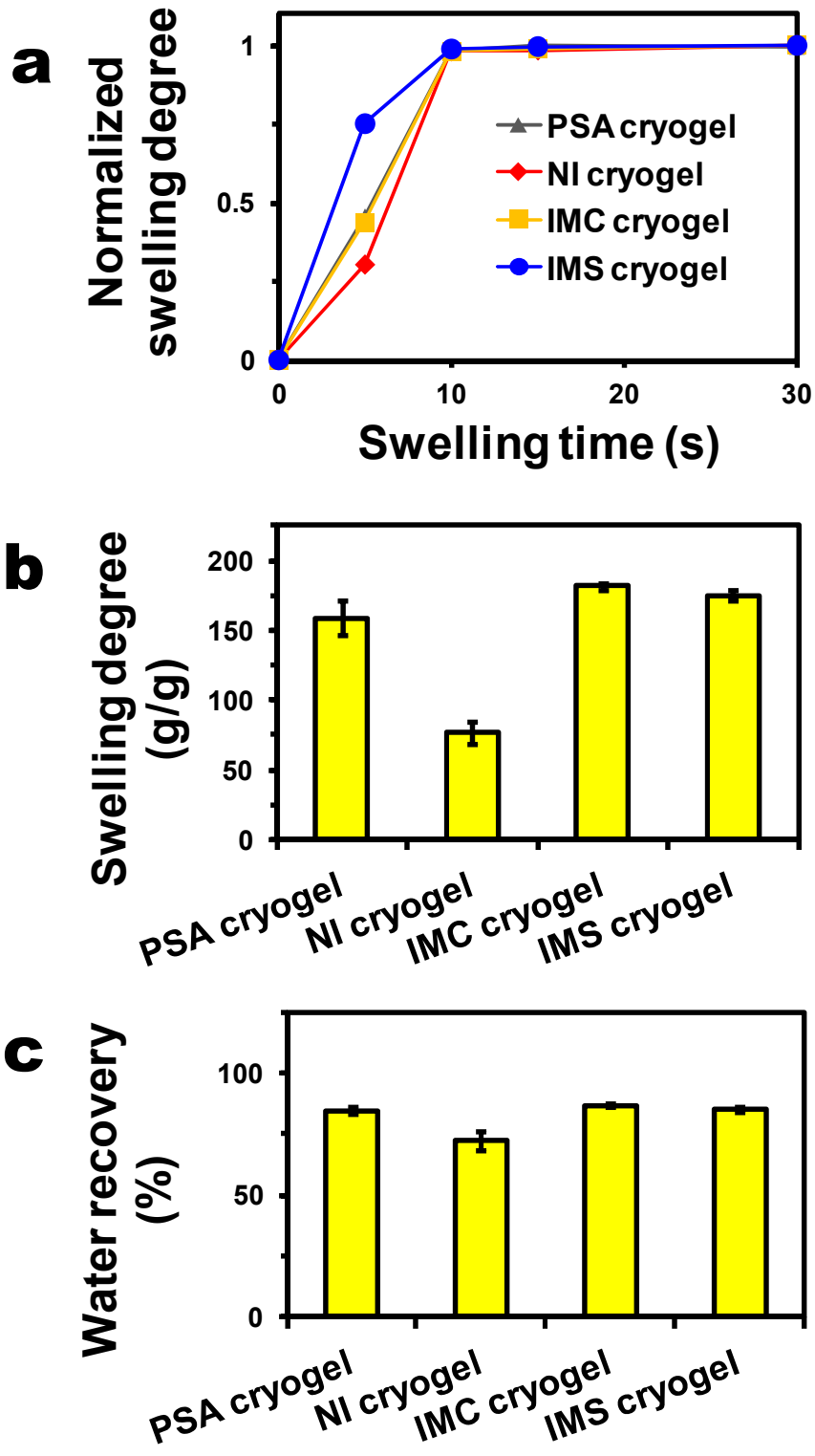

Fig. 5 (a) Swelling profile, (b) equilibrium swelling degree, and (c) water recovery efficiency of cryogels prepared via different methods.

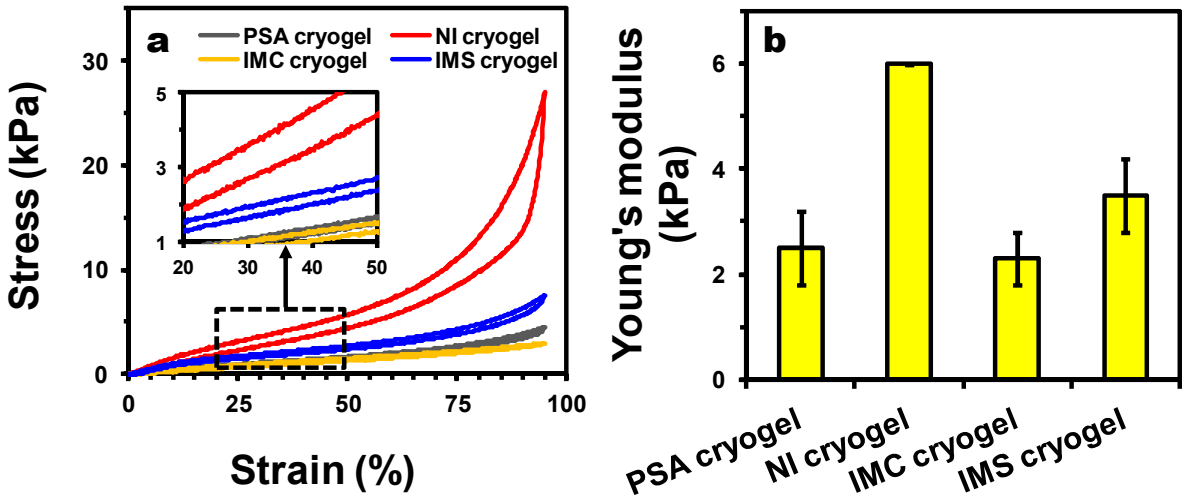

Fig. 6 (a) Stress-strain curve and (b) Young's modulus of the AgNP-incorporated cryogels prepared via different methods. Note: Young's modulus was determined by taking the initial slope of the stress-strain curves (n=3).

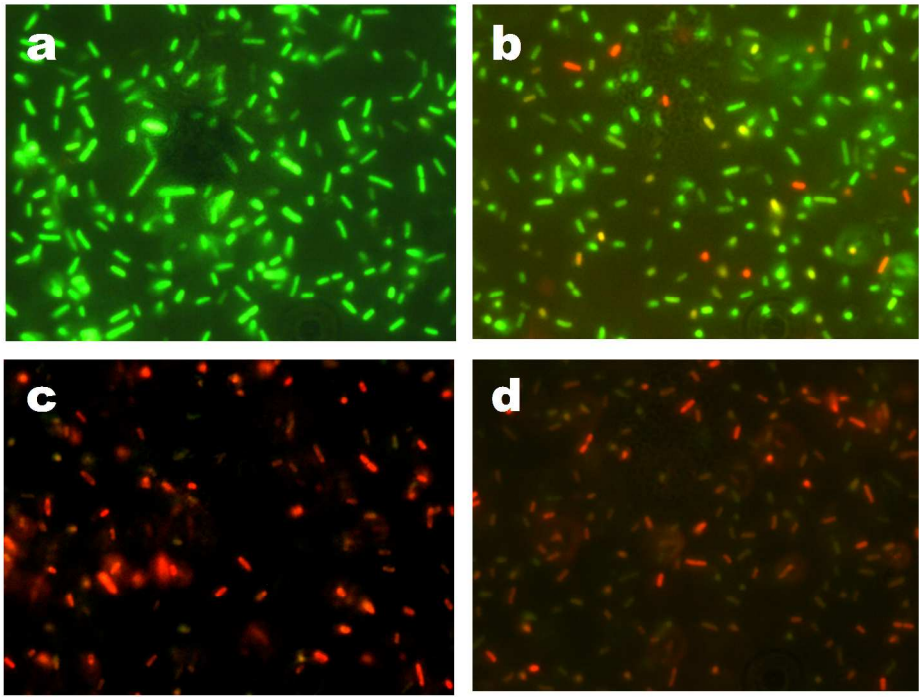

Fig. 7 Representative fluorescence images of bacterial samples exposed to (a) PSA cryogels, (b) NI cryogels, (c) IMC cryogels, and (d) IMS cryogels. Note: live cells fluoresce green while membrane-compromised cells fluoresce red.

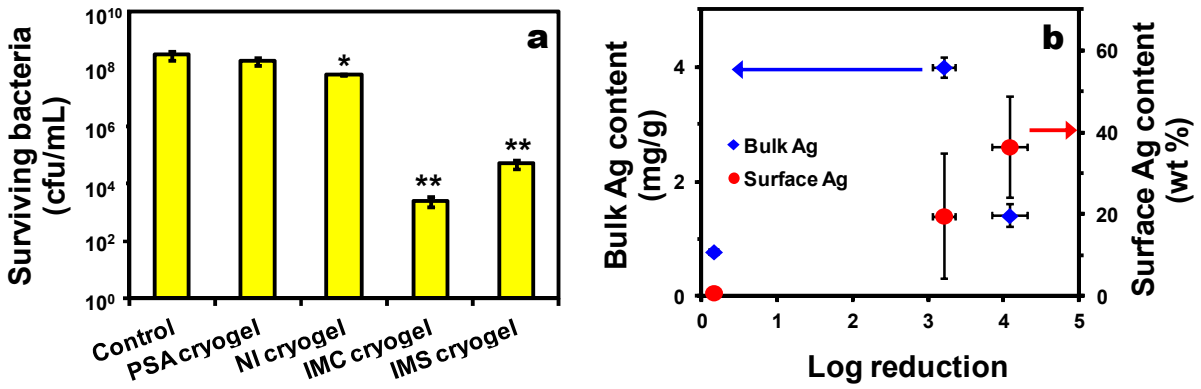

Fig. 8 (a) Number of viable bacteria in water samples exposed to various AgNP-incorporated cryogels. Note that (*) and (**) denote significantly different results (based on Student's *t*-test; n=6) compared to control at 95% and 90% confidence levels, respectively. (b) Relationship between the disinfection efficacies and the bulk and surface Ag content. Note: the bulk Ag content was determined by ICP-OES analyses of acid-digestion of the cryogel nanocomposites, while the surface Ag content was estimated using EDX analyses of at least 3 sites for each cryogel sample.

TOC Art

AgNPs-incorporated cryogels prepared via three synthesis routes were explored as antibacterial sorbents for water disinfection